DISTURBED STRESS FIELD MODEL FOR REINFORCED CONCRETE: IMPLEMENTATION

By F. J. Vecchio[1]

ABSTRACT: The Disturbed Stress Field Model is a smeared delayed-rotating-crack model, proposed recently as an alternative to fully fixed or fully rotating crack models, for representing the behavior of cracked reinforced concrete. It is an extension of the modified compression field theory; advancements relate to the inclusion of crack shear slip in the element compatibility relations, the decoupling of principal stress and principal strain directions, and a revised look at compression softening and tension stiffening mechanisms. In this paper, a procedure is described for implementing the formulations of the Disturbed Stress Field Model into a nonlinear finite-element algorithm. The procedure is based on a total-load secant-stiffness approach, wherein the crack slip displacements are treated as offset strains. Computational aspects of the formulation are shown to be simple and numerically robust. The hybrid crack slip formulation used is found to accurately model the divergence of stress and strain directions, providing an improved representation of behavior. Predictions of shear strength and failure mode are significantly influenced in some cases.

INTRODUCTION

The Disturbed Stress Field Model (DSFM) was introduced in Vecchio (2000) as an alternative formulation for describing the behavior of cracked reinforced concrete elements. The theory is an extension of the modified compression field theory (MCFT) (Vecchio and Collins 1986), with advancements made primarily with respect to modeling of shear slip along cracks. The impetus was to address the diminished accuracy seen from existing procedures under certain conditions, particularly for beams or wall elements containing no shear reinforcement. The new formulation combines aspects of rotating-crack and fixed-crack models, giving an improved representation of crack mechanisms and thereby resulting in increased accuracy.

In the DSFM formulation presented in Vecchio (2000), material response is described at a fundamental (element) level for membranes subjected to general 2D stress conditions. Particular attention is given to including crack shear slip in the description of the element's distortion; new equilibrium, compatibility, and constitutive relations are defined accordingly. Compatibility relations are defined such that, given the element's total (apparent) strain condition $[\varepsilon]$, the concrete deformations are resolved into components representing elastic strain due to stress $[\varepsilon_c]$, equivalent average strain due to rigid slip along the crack surfaces $[\varepsilon^s]$, elastic offset strains $[\varepsilon_c^0]$ due to mechanisms such as thermal expansion or shrinkage, and plastic offset strains $[\varepsilon_c^p]$ due to mechanisms relating to loading history and material damage. Thus, for the concrete component, the compatibility relation is

$$[\varepsilon] = [\varepsilon_c] + [\varepsilon^s] + [\varepsilon_c^0] + [\varepsilon_c^p] \tag{1}$$

From the elastic strains due to stress $[\varepsilon_c]$, standard strain transformations are used to determine concrete principal strains, angle of inclination of the stress field, and crack direction. Note that the angle of inclination thus determined will differ from the angle of inclination of the total strains, eliminating the requirement previously held in the MCFT that the inclinations of principal stress and principal strain coincide.

Also described in Vecchio (2000) are constitutive relations for cracked reinforced concrete. These are largely based on the formulations previously presented for the MCFT, which in themselves were based on the results of extensive experimental investigations. The MCFT relations were revised somewhat, however, to reflect the new view of crack slip taken in the DSFM. Thus, given the net (elastic) principal strains in the concrete, calculations of the concrete principal stresses can be made. Material and element stiffness factors can then be defined according to the analysis approach being adopted.

This paper shows how the conceptual model and analytical relations of the DSFM can be incorporated into a nonlinear finite-element algorithm. An example analysis is used to demonstrate the formulation of the model and numerical aspects of the solution algorithm. A general discussion is then given identifying important behavior models implicit in the theory and how they differ from alternative formulations. Finally, example analyses are presented illustrating application of the analysis procedure and the significance it has on the computed response.

FINITE-ELEMENT IMPLEMENTATION

Consider the state of stress and strain at a point in a reinforced concrete continuum, as shown in Fig. 1. Given a stress $[\sigma]$ acting at the point, the resulting total strain $[\varepsilon]$ will be such as to satisfy the condition

$$[\sigma] = [D][\varepsilon] - [\sigma^0] \tag{2}$$

where $[D]$ = composite material stiffness matrix. The element pseudo-prestress $[\sigma^0]$, due to elastic and plastic strain offsets in the concrete and reinforcement (including crack shear slip), is defined as follows:

$$[\sigma^0] = [D_c]\{[\varepsilon^s] + [\varepsilon_c^0] + [\varepsilon_c^p]\} + \sum_{i=1}^{n} [D_s]_i[\varepsilon_s^0]_i \tag{3}$$

For the implementation procedure described here, the material stiffness matrix $[D]$ for a reinforced concrete element will be constructed in the context of a secant-stiffness formulation. Stiffness matrices for the concrete $[D_c]'$ and each of the reinforcement components $[D_s]_i'$ are first defined with respect to their principal axes. The total stiffness is then determined by combining the contributions from each of the components, using appropriate transformations to account for anisotropy.

Cracked concrete is treated as an orthotropic material with its principal axes (1,2) corresponding to the direction of the average principal stresses (i.e., crack direction). In defining secant stiffness values, net strains $[\varepsilon_c]$ are used; that is, total strains $[\varepsilon]$ less strains due to crack slip $[\varepsilon^s]$, elastic offsets

[1]Prof., Dept. of Civ. Engrg., Univ. of Toronto, Toronto, Canada M5S 1A4.

Note. Associate Editor: Julio Ramirez. Discussion open until June 1, 2001. To extend the closing date one month, a written request must be filed with the ASCE Manager of Journals. The manuscript for this paper was submitted for review and possible publication on November 19, 1999. This paper is part of the ***Journal of Structural Engineering***, Vol. 127, No. 1, January, 2001. ©ASCE, ISSN 0733-9445/01/0001-0012–0020/$8.00 + $.50 per page. Paper No. 22148.

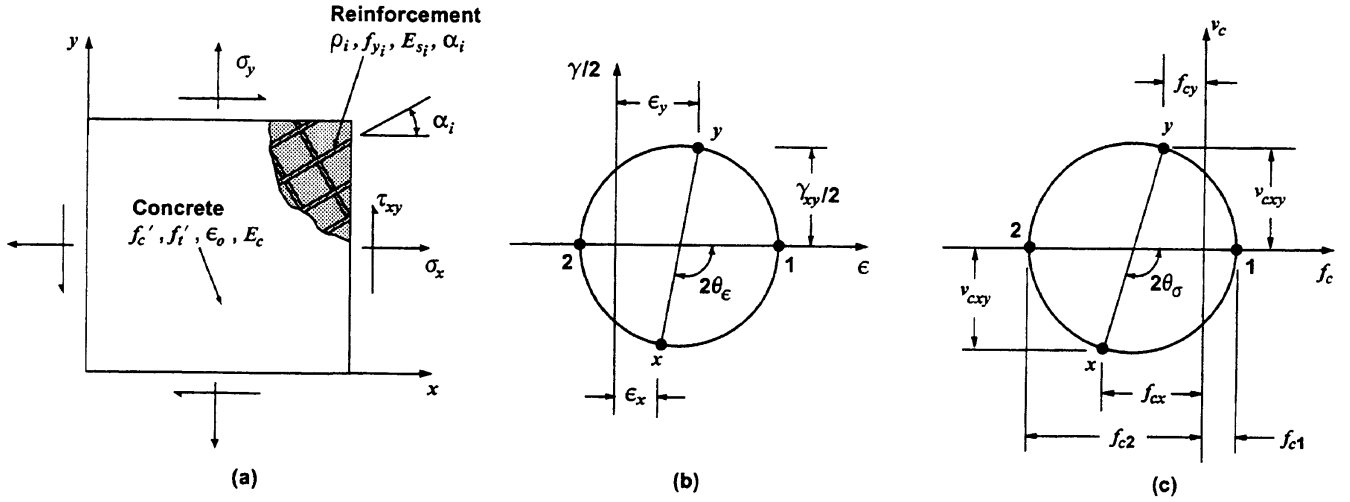

FIG. 1. Reinforced Concrete Element: (a) Element Properties and Applied Stresses; (b) Total Average Strain Conditions in Element; (c) Average Stresses in Concrete

$[\epsilon_c^0]$, and plastic offsets $[\epsilon_c^p]$. Hence, the concrete material stiffness matrix $[D_c]'$, evaluated relative to the principal stress directions (1,2), is

$$[D_c]' = \begin{bmatrix} \bar{E}_{c1} & 0 & 0 \\ 0 & \bar{E}_{c2} & 0 \\ 0 & 0 & \bar{G}_c \end{bmatrix} \tag{4}$$

where $\bar{E}_{c1}$, $\bar{E}_{c2}$, and $\bar{G}_c$ = secant moduli. At a particular stress-strain state, the secant moduli are evaluated as follows:

$$\bar{E}_{c1} = \frac{f_{c1}}{\epsilon_{c1}}; \quad \bar{E}_{c2} = \frac{f_{c2}}{\epsilon_{c2}}; \quad \bar{G}_s = \frac{\bar{E}_{c1} \cdot \bar{E}_{c2}}{\bar{E}_{c1} + \bar{E}_{c2}} \tag{5}$$

where ϵ_{c1} and ϵ_{c2} = net principal strains in the concrete; and f_{c1} and f_{c2} = corresponding principal stresses [Fig. 2(a)]. Poisson's effects and lateral expansion, if being considered, are treated in the manner of elastic offsets $[\epsilon_c^0]$.

For each reinforcement component, a corresponding matrix $[D_s]_i'$ is evaluated

$$[D_s]_i' = \begin{bmatrix} \rho_i \bar{E}_{s_i} & 0 & 0 \\ 0 & 0 & 0 \\ 0 & 0 & 0 \end{bmatrix} \tag{6}$$

where ρ_i = reinforcement ratio. The secant modulus $\bar{E}_{s_i}$ is defined

$$\bar{E}_{s_i} = \frac{f_{s_i}}{\epsilon_{s_i}} \tag{7}$$

where ϵ_{s_i} and f_{s_i} = average strain and average stress, respectively, in the reinforcement [Fig. 2(b)].

The component material stiffness matrices are transformed to the global reference system and then summed. The total material stiffness matrix $[D]$ is evaluated

$$[D] = [D_c] + \sum_{i=1}^{n} [D_s]_i \tag{8}$$

where

$$[D_c] = [T_c]^T [D_c]' [T_c] \tag{9}$$

$$[D_s]_i = [T_s]_i^T [D_s]_i' [T_s]_i \tag{10}$$

The transformation matrix $[T]$ is given by

$$[T] = \begin{bmatrix} \cos^2\psi & \sin^2\psi & \cos\psi \sin\psi \\ \sin^2\psi & \cos^2\psi & -\cos\psi \sin\psi \\ -2\cos\psi \sin\psi & 2\cos\psi \sin\psi & (\cos^2\psi - \sin^2\psi) \end{bmatrix} \tag{11}$$

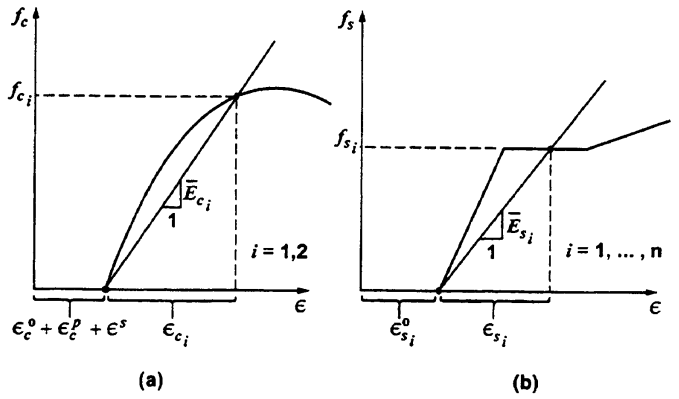

FIG. 2. Definition of Secant Moduli: (a) Concrete; (b) Reinforcement

where $\psi = \theta$ for the concrete (i.e., inclination of principal stress); and $\psi = \alpha_i$ for the reinforcement (i.e., orientation of bars).

In this formulation, it is necessary to account for the strain offsets in determining prestrain nodal forces. For the crack slip strains $[\epsilon^s]$, free joint displacements $[r_c^s]$ are determined from the element geometry; that is

$$[r_c^s] = \int [\epsilon^s] \, dA \tag{12}$$

Given the free displacements, the prestrain joint forces $[F_c^s]$ can be evaluated

$$[F_c^s] = [k_c][r_c^s] \tag{13}$$

where $[k_c]$ = concrete component of the element stiffness matrix. Prestrain forces are similarly calculated for the elastic and plastic offset strains. The prestrain forces are then added to the nodal load vector. A full description of the approach is given in Vecchio (1992).

A total-load, iterative secant-stiffness routine is then used to perform a nonlinear analysis for a reinforced concrete structure. Through each iteration, the material stiffness $[D]$ and element stiffness $[k]$ matrices are progressively refined until satisfactory convergence is achieved. The convergence criteria can be based on either the secant moduli or the element displacements achieving stable values. A flow chart and description of the algorithm was given by Vecchio (1990) for elements with elastic offsets only; the plastic and shear slip offsets are treated in an analogous manner. A subportion of the algorithm that will be useful in performing a sample cal-

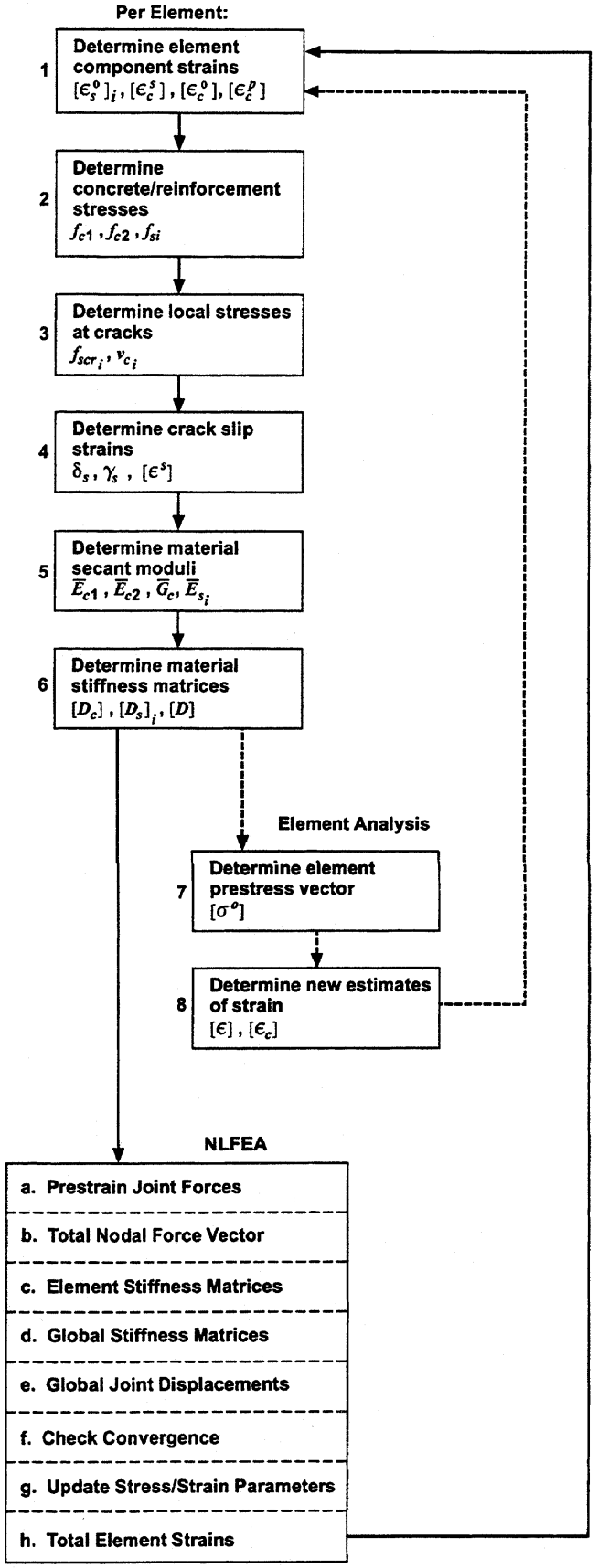

FIG. 3. Nonlinear Analysis Algorithm

culation is shown in Fig. 3. In this regard, it should be noted that, as the stiffness matrices change through each iteration, so too will the prestrain force vectors due to crack slip strains, elastic offsets, and plastic offsets. Hence, the total force vectors must be recalculated through each iteration.

EXAMPLE SOLUTION

As an illustration of the calculations involved, consider Panel PV19 (Vecchio and Collins 1982). The material properties of the panel are as follows: f'_c = 19.0 MPa; f'_t = 1.72 MPa, $\varepsilon_0 = -0.00215$, a = 10 mm, $\rho_x = 0.01785$, $\rho_y = 0.00713$, f_{yx} = 458 MPa, f_{yy} = 300 MPa, and E_s = 200,000 MPa. An analysis will be performed for the uniform loading condition of σ_x = 0 MPa, σ_y = 0 MPa, and τ = 3.0 MPa. For the sake of simplicity, it will be assumed that there are no elastic offsets, including no postcracking Poisson effects, and no plastic offsets. From available crack spacing models (e.g., CEB-FIP model code), the spacing of cracks in the x- and y-directions (s_x and s_y) are estimated to be approximately 50 mm.

In the first cycle of calculations, using the stiffness factors and shear slip strains carried over from the previous load stage (τ = 2.9 MPa), total strains are determined to be $[\varepsilon] = \{0.607\ \ 1.159\ \ 2.302\} \times 10^{-3}$. After 10 iterations of the solution algorithm, total apparent strains in the element change to $[\varepsilon] = \{0.597\ \ 1.208\ \ 2.338\} \times 10^{-3}$. Given in Appendix I are the calculations that result during the 11th iteration. Note, in particular, the calculation of the crack slip strains; at this stress level, the stress-based criterion governs. Strains calculated during this iteration are found to be $[\varepsilon] = \{0.596\ \ 1.209\ \ 2.339\} \times 10^{-3}$. Although the strains appear to have converged, there remains some change in the computed inclination of the stress field; hence, additional iterations are required. After 20 iterations, all values have stabilized and the resulting strains are $[\varepsilon] = \{0.594\ \ 1.216\ \ 2.342\} \times 10^{-3}$. Note that all calculations involved are simple in nature and convergence is rapid and stable.

SHEAR SLIP MODEL

In the DSFM formulation, various alternatives were considered for modeling crack shear slip. One was to employ an explicit constitutive model to relate the amount of shear slip along the crack to the magnitude of the shear stress acting on the crack. A second alternative was to fix the degree of "lag" between the rotation of the stress field in the concrete and that of the strain field. For reasons previously discussed, a hybrid approach was taken combining the two.

For the stress-based approach, the relationship adopted was that of Walraven (1981), taking the stiffness portion of this model as follows:

$$\delta_s = \frac{v_{ci}}{1.8w^{-0.8} + (0.234w^{-0.707} - 0.20)\cdot f_{cc}} \tag{14}$$

where δ_s = slip displacement along the crack (mm); v_{ci} = shear stress acting on the crack (MPa); w = average crack width (mm); and f_{cc} = concrete cube strength (MPa). An alternative formulation is obtained by drawing on the work of Okamura and Maekawa (1991). Defining $v_{c\max}$ as the maximum shear stress that can be resisted on the crack and a as the aggregate size in millimeters, the following shear slip relation is obtained:

$$\delta_s = \frac{3}{4} w \sqrt{\frac{\psi}{\psi - 1}} \tag{15}$$

where

$$\psi = v_{ci}/v_{c\max} \tag{16}$$

$$v_{c\max} = \frac{\sqrt{f'_c}}{0.31 + 24w/(a + 16)}\ \text{(MPa)} \tag{17}$$

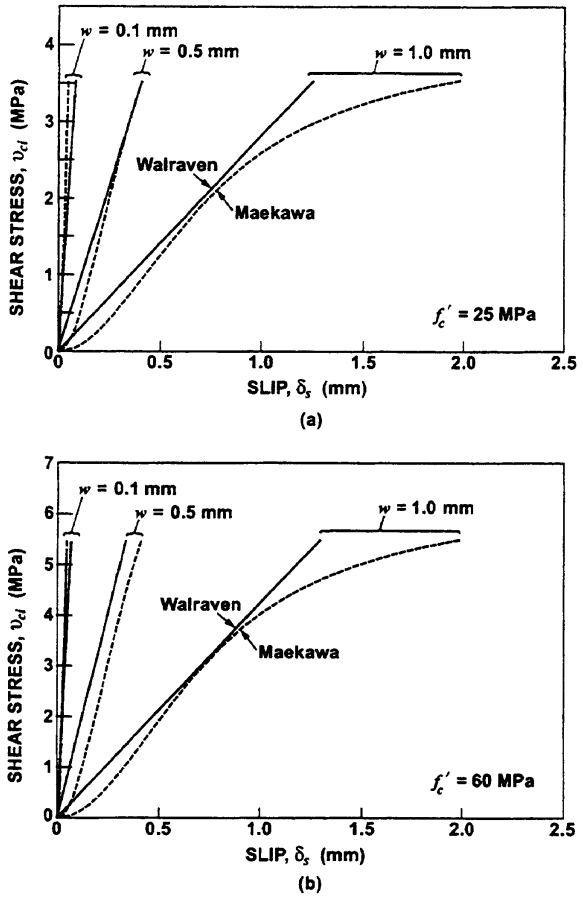

FIG. 4. Comparison of Concrete Shear-Stress–Shear-Slip Models: (a) for 25 MPa Concrete; (b) for 60 MPa Concrete

As shown in Fig. 4, the two stress-based formulations provide essentially similar stiffnesses, although they differ somewhat in representing the initial slip.

To assess sensitivity to the various slip models and provide an opportunity for comparison to the MCFT formulation, consider again the response of Panel PV19. Separate analyses were performed using, alternatively, the rotation lag, crack shear stress, and hybrid criteria for crack shear slip. Shown in Fig. 5(a) are the resulting computed shear-stress–shear-strain responses. There are only minor differences among the three DSFM simulations, with the rotation lag approach giving very slightly increased deformations at the early stages and the stress-based formulation giving a reduced strength and stiffness at the intermediate stages of loading. The hybrid formulation provides a smooth transition between the two, producing a result that agrees reasonably well with the experimental values. The MCFT formulation also gives a good representation of response, although the deformation at the ultimate load stage is significantly underestimated. More importantly, there is a subtle but meaningful difference in the predicted failure mode. The MCFT predicts failure by the concrete stress attaining its peak strength, $f_{c2} > f_p$ (i.e., concrete crushing). The DSFM, on the other hand, indicates behavior governed by excessive slip along the crack surface leading to a concrete shear failure. The latter is more consistent with the observed failure mode.

For this same set of analyses, the predicted angles of inclination of the stress and strain fields are shown in Figs. 5(b and c), respectively. Here, the differences between the various formulations become more apparent. The hybrid formulation for the crack shear slip provides a reasonably good representation of the response measured in the test panel, particularly at load stages near ultimate where the inclination of the apparent strain field begins to increase rapidly. The other two slip formulations also provide good agreement. The MCFT formulation, on the other hand, assumes that the two angles of inclination are equal; the values computed lie approximately midway between the inclination of the principal strains and that of the principal stresses, significantly misrepresenting both.

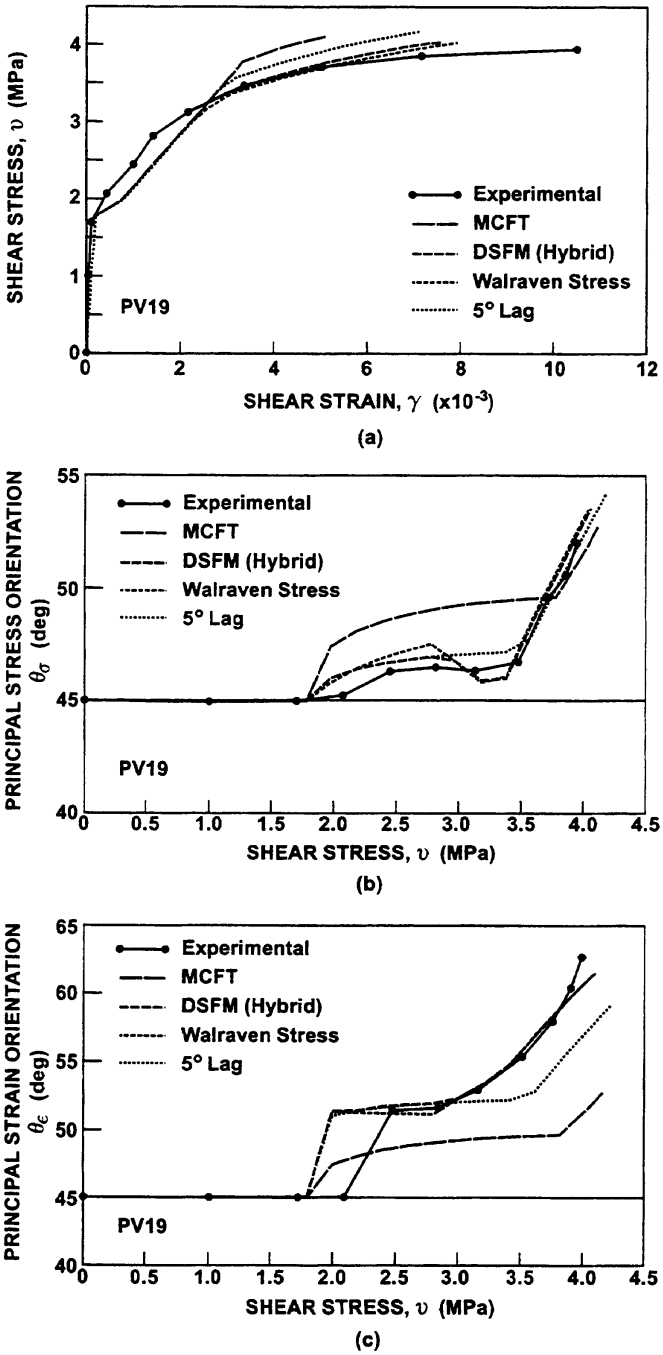

FIG. 5. Comparison of Experimental and Theoretical Responses for Panel PV19: (a) Shear Stress-Strain Response; (b) Inclination of Principal Stress Direction; (c) Inclination of Apparent Principal Strain Direction

SHEAR STRENGTH

Analyses were performed for a hypothetical panel in which the longitudinal reinforcement was fixed at $\rho_x = 2.5\%$ and the transverse reinforcement ratio was increased from $\rho_y = 0\%$ to $\rho_y = 3\%$. The remaining material properties were held constant: $f_c' = 25$ MPa, $f_t' = 2.0$ MPa, $\varepsilon_0 = -0.002$, $a = 15$ mm, $s_x = s_y$

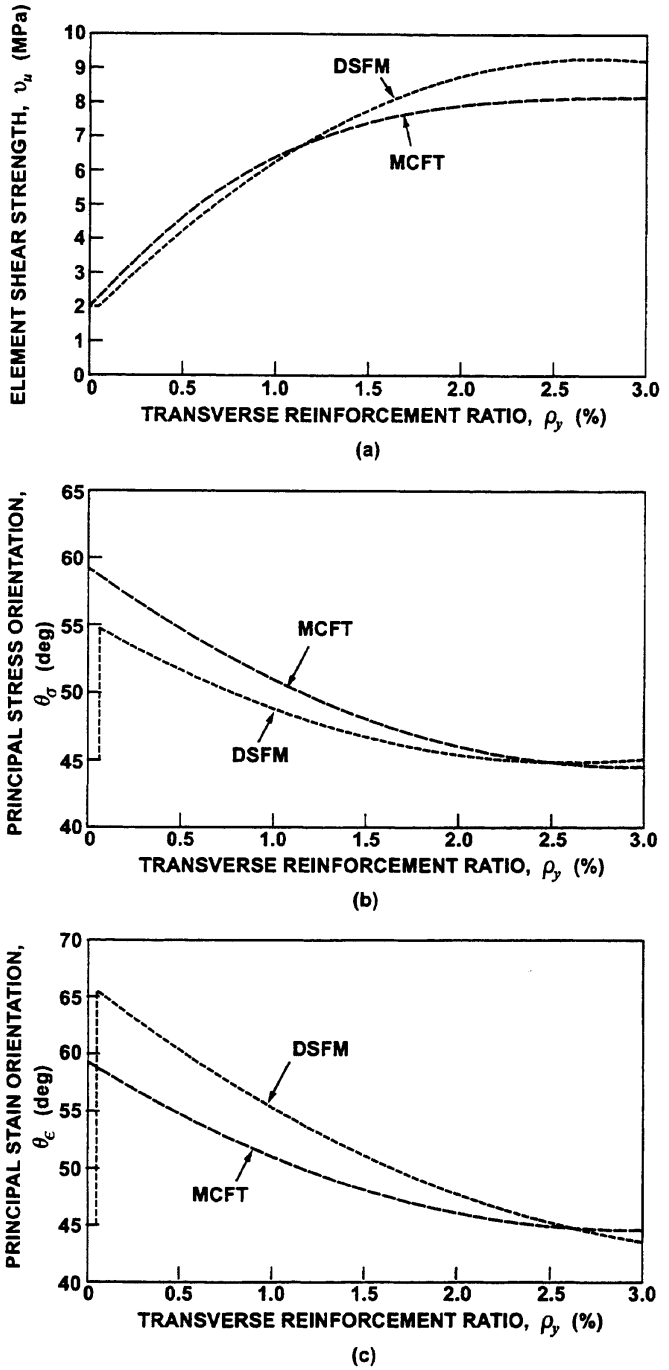

FIG. 6. Comparison of Predicted Responses for Hypothetical Panel: (a) Shear Capacity; (b) Inclination of Principal Stresses at Ultimate Load; (c) Inclination of Principal Strains at Ultimate Load

= 50 mm, $f_{yx} = f_{yy}$ = 450 MPa, and E_s = 200,000 MPa. Shown in Fig. 6(a) are the ultimate shear strengths of the panel as predicted by the DSFM (hybrid model) and MCFT. At low values of transverse reinforcement ratio, the DSFM predicts shear capacities approximately 10% lower than those obtained using the MCFT. Note in particular that, for transverse reinforcement levels of 0.05% or less, capacity is dictated by the stress at first cracking (i.e., shear strength is constant). At high reinforcement ratios and in situations where there is little slip induced on the crack (e.g., $\rho_x \approx \rho_y$), shear strengths predicted by the DSFM are significantly higher. This is more consistent with observed test results; for example, with panels PV23 and PV25 (Vecchio and Collins 1982) and panels tested by Kollegger and Mehlhorn (1990).

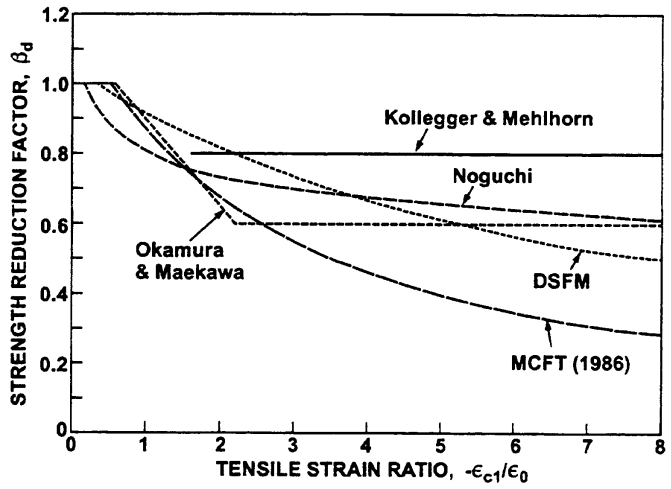

FIG. 7. Comparison of Alternative Models for Compression Strength Reduction due to Transverse Cracking

Shown in Figs. 6(b and c) are the corresponding orientation of the stress and strain fields. At low transverse reinforcement levels, the DSFM predicts angles of inclination for the principal tensile strain approximately 8° higher than those predicted by the MCFT. For the inclination of the principal tensile stress, normal to the crack direction, the DSFM angle of orientation is about 4° lower. These differentials can be significant in situations where the flow of force from the load application point to the supports may or may not form a direct strut (i.e., in beams with short shear spans). As the transverse reinforcement level increases, differences diminish to zero.

A comment is also in order regarding the substantially reduced degree of compression softening included in the new formulation. Inclusion of crack shear slip in the compatibility relations of the DSFM results in reduced element stiffness. Hence, less stiffness degradation need be ascribed to the softening of the concrete in compression due to the influence of transverse cracks. In the MCFT, where deformations due to crack slip are not explicitly considered, the necessary degradation in element stiffness is represented entirely by an increased compression softening factor. In this regard, the DSFM approach is more rational and more consistent with the degree of compression softening reported by other researchers (Fig. 7). However, the two approaches yield substantially similar results over a wide range of problems, as demonstrated in Fig. 6(a) discussed above. Difficulties will arise only if the two formulations are incorrectly combined [for example, using the softening equations of the MCFT with the compatibility relations of the DSFM (or other crack slip models or fixed-crack models) or using reduced softening formulations in fully rotating crack (i.e., MCFT-like) models].

SAMPLE APPLICATION

To illustrate the theoretical model's application to the analysis of reinforced concrete structures through nonlinear finite-element procedures, an analysis was made of a concrete box structure recently tested at the University of Toronto by Kuzmanovic (1998). The structural details of the test specimen are given in Fig. 8; note that the walls of the structure contain no shear reinforcement. The model was loaded at several points by actuators acting on the top and bottom walls, simulating soil pressures acting on the external surfaces. The load was monotonically increased until a brittle shear failure occurred in the top slab, near the slab-wall joint, at a load equivalent to a uniformly distributed load of 350 kN/m^2.

The finite-element model constructed to represent the test specimen is shown in Fig. 9(a). A total of 788 8-degrees-of-

freedom (DOF) rectangular elements and 4 6-DOF triangular elements were used to present the concrete sections. Longitudinal reinforcement was mostly modeled as smeared within appropriate narrow bands of elements, although 44 truss bar elements were used to augment the modeling to properly represent the reinforcement details. Analyses were conducted using a load increment of 10 kN/m^2. The nonlinear finite-element analysis (NLFEA), utilizing the formulations of the DSFM, found the structure to withstand an ultimate load of 370 kN/m^2. Failure occurred by shear failure of the top slab, near the corner, as in the test specimen. The observed and calculated load-deflection responses of the specimen are compared in Fig. 9(b). It is seen that the predicted response is somewhat stronger, more flexible, and more ductile than that observed. However, given that this is a large-scale shear-critical structure containing no shear reinforcement, the correlation is of acceptable accuracy; such structural elements are prone to wide scatter in their responses (Vecchio 1999). It should be noted that the calculated flexural capacity of the structure is 635 kN/m^2 and the American Concrete Institute code calculated shear capacity is 455 kN/m^2.

A more typical application of the analysis procedure would be one where the structure contains at least minimum reinforcement (for example, a shear wall structure). Considered here is Wall SW16, tested by Lefas et al. (1990), shown in Fig. 10. The wall web region contained 1.1% horizontal and 2.1% vertical reinforcements. The concealed column elements at the edges of the wall contained 3.1% vertical reinforcement and also hoop ties representing an out-of-plane reinforcement level of 1.2%. The test specimen was subjected to a monoton-

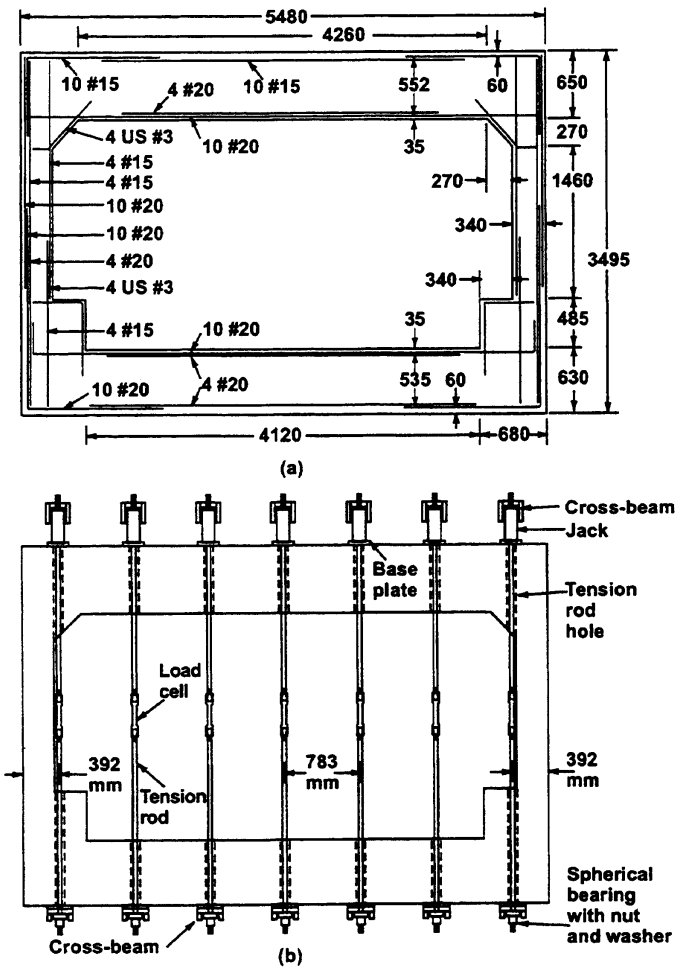

FIG. 8. Details of Box Structure Tested by Kuzmanovic (1998)

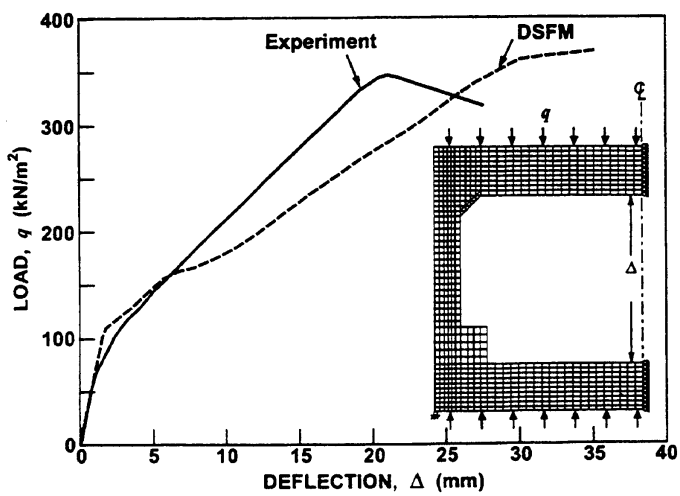

FIG. 9. Comparison of Experimental and Calculated Load-Deflection Response of Kuzmanovic Box Structure

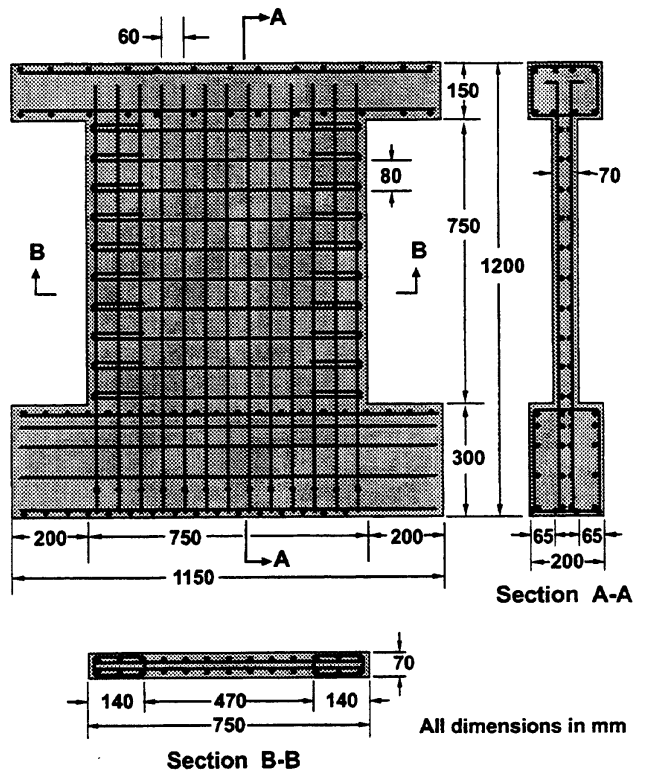

FIG. 10. Details of Wall SW16 Tested by Lefas et al. (1990)

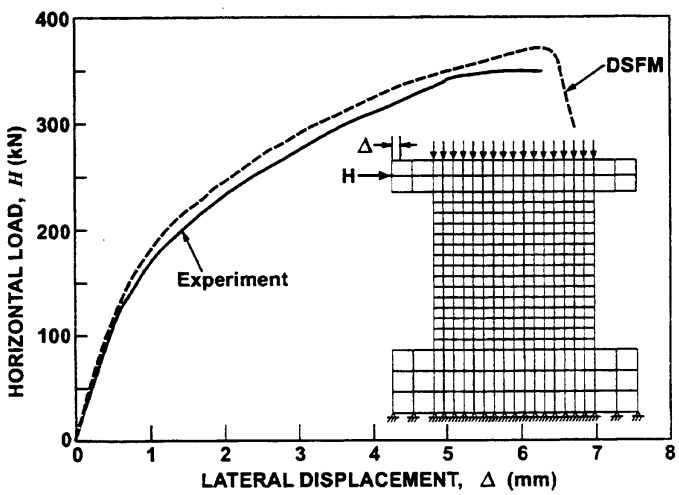

FIG. 11. Results of Finite-Element Analysis of Wall SW16

ically increasing lateral load in combination with a constant axial load. Wall SW16 was a well-reinforced and confined squat wall; its ultimate capacity and deflection response were shear critical and influenced by confinement effects.

The wall specimen was represented by the finite-element model shown in Fig. 11(a) comprising 340 8-DOF rectangular elements. Lateral load was applied as a monotonically increasing imposed displacement in 0.2-mm increments. The resulting load-deflection response at the top beam level is shown in Fig. 11(b). The computed lateral load capacity of 365 kN compares well with the experimentally determined value of 350 kN. As well, the stiffness and ductility of the wall are accurately represented. The predicted failure mode, involving a shear-crushing failure in the compression-toe region of the wall, is also consistent with the observed behavior.

CONCLUSIONS

The DSFM, for analysis of reinforced concrete elements, is presented in a form adaptable to nonlinear finite-element algorithms. Procedures are described for implementation into a total-load, secant-stiffness based formulation. Crack shear slip as well as other elastic and plastic offset strains in the concrete and reinforcement are handled through use of prestrain nodal forces. The resulting algorithm is stable and robust, allowing calculation of an element's load-deformation response up to and beyond ultimate capacity. The conceptual model is simple and transparent, and the calculations involved are basic.

The sample problem and investigative studies undertaken yielded the following observations:

- The presented crack slip formulations allow for the divergence of principal stress and principal strain directions in the concrete, providing a better representation of typical behavior observed in test specimens.
- The described hybrid crack slip model is a successful amalgamation of stress-based and lag-based approaches; however, the stress-based slip model taken alone is sufficient in most applications.
- In elements containing little or no transverse reinforcement, the rotation of the concrete stress field is retarded by up to 10° relative to that of the strain field, resulting in reduced computed shear capacities compared to those obtained from a fully rotating crack model where the inclination of the stress and strain fields are assumed to coincide.
- In elements containing high amounts of shear reinforcement, the lower degree of compression softening ascribable to transverse cracking results in considerably increased shear capacities relative to those obtained according to the fully rotating crack model.
- The degree of compression softening required in the delayed-rotating-crack model (DSFM) is consistent with that reported by other researchers.

A thorough corroboration of the accuracy of the proposed formulation is possible (Vecchio, unpublished manuscript, 2000).

APPENDIX I. SAMPLE CALCULATIONS

Consider Panel PV19, with properties as previously described, subjected to a pure shear load of $\tau_{xy} = 3.0$ MPa. Response is calculated according to the formations presented, using the secant-stiffness algorithm summarized in Fig. 3 (at the element level). For simplicity, it will be assumed that elastic expansion offsets $[\varepsilon_c^0]$ and plastic offsets due to loading history and material flow $[\varepsilon_c^p]$ are zero. Elastic offsets in the reinforcement $[\varepsilon_s^0]_i$ are also zero.

At the current load stage, after 10 iterations of the iterative procedure, the total apparent strains $[\varepsilon]$ and concrete net strains $[\varepsilon_c]$ are found to be

$$[\varepsilon] = \{0.597 \quad 1.208 \quad 2.338\} \times 10^{-3}$$

$$[\varepsilon_c] = \{0.823 \quad 0.982 \quad 2.377\} \times 10^{-3}$$

Calculations will now be performed for the 11th iteration.

Note that equation numbers prefixed with I [e.g., Eq. (I-33)] refer to equations given in Vecchio (2000).

Step 1: Strain Components

1. Using Eqs. (I-10) and (I-11), determine the average principal strains and their inclination

$$\varepsilon_{c1} = 2.094 \times 10^{-3}, \quad \varepsilon_{c2} = -0.288 \times 10^{-3}; \quad \theta_\sigma = 46.92°$$

2. For inclination of apparent strains, use Eq. (I-9)

$$\theta_\varepsilon = 52.34°$$

3. For average strains in reinforcement, use Eq. (I-19)

$$\varepsilon_{sx} = 0.597 \times 10^{-3}; \quad \varepsilon_{sy} = 1.208 \times 10^{-3}$$

Step 2: Average Stresses in Concrete and Reinforcement

1. From Eq. (I-24), find $C_d = 1.658$. Given that $C_s = 0.55$, use Eq. (I-23) to calculate $\beta_d = 0.523$. Hence, using Eqs. (I-26) and (I-27), find $f_p = -9.94$ MPa and $\varepsilon_p = -1.124 \times 10^{-3}$. Using the Popovic's formulation [Eqs. (I-28)–(I-30)] find

$$f_{c2} = -4.93 \text{ MPa}$$

2. Average principal tensile stress in concrete—from the tension softening mechanisms, using Eqs. (I-33) and (I-34) and assuming $G_f = 7.5$ N/m, $L_{ref} = 750$ mm, and $f_t' = 1.72$ MPa, find

$$f_{c1}^a = 0.00 \text{ MPa}$$

From the tension stiffening mechanisms, using Eqs. (I-35)–(I-37), find

$$f_{c1}^b = 1.08 \text{ MPa}$$

Hence, using Eq. (I-38), find

$$f_{c1} = \max(f_{c1}^a, f_{c1}^b) = 1.08 \text{ MPa}$$

3. Average stresses in reinforcement—from the average strains ε_{sx} and ε_{sy}, using Eq. (I-39), find

$$f_{sx} = 119 \text{ MPa}; \quad f_{sy} = 242 \text{ MPa}$$

Step 3: Local Stresses at Cracks

1. To satisfy equilibrium Eq. (I-7), using an iterative procedure, find the incremental strain at the crack to be $\Delta\varepsilon_{1cr} = 1.111 \times 10^{-3}$. Hence, using Eq. (I-20), calculate local rebar strains

$$\varepsilon_{scr_x} = 1.115 \times 10^{-3}; \quad \varepsilon_{scr_y} = 1.802 \times 10^{-3}$$

Using Eq. (I-39), find local rebar stresses

$$f_{scr_x} = 223 \text{ MPa}; \quad f_{scr_x} = 300 \text{ MPa}$$

Check the equilibrium

$$\sum \rho_i(f_{scr_i} - f_{s_i})\cos^2\theta_{n_i} = (0.01785)(223 - 119)\cos^2(46.92°)$$

$$+ (0.00713)(300 - 242)\cos^2(-43.08°) = 1.08 \text{ MPa} = f_{c1}$$

2. Find the shear stress on the crack using Eq. (I-8)

$$v_{ci} = 0.716 \text{ MPa}$$

Step 4: Crack Slip

1. Calculate the crack spacing, from Eq. (I-21), to be s = 35.4 mm. Calculate the crack width, using Eq. (I-22), to be w = 0.073 mm
2. From the stress-based approach, using Eqs. (I-40) and (I-12), calculate the shear slip strain

$$\gamma_s^a = 0.460 \times 10^{-3}$$

3. From the rotation lag approach, using an initial crack direction of $\theta_{ic} = 45°$ and the lag limit $\theta^{\ell} = 5°$, find from Eqs. (I-41)–(I-43) that

$$\Delta\theta_\varepsilon = 7.34°; \quad \Delta\theta_\sigma = 2.34°$$

And hence, $\theta_\sigma = 47.34°$. Now, using Eq. (I-18), find

$$\gamma_s^b = 0.418 \times 10^{-3}$$

4. At this stage of loading, the stress-based criterion governs

$$\gamma_s = \max(\gamma_s^a, \gamma_s^b) = 0.460 \times 10^{-3}$$

5. Resolve the slip strain into orthogonal components using Eqs. (I-13)–(I-15)

$$\varepsilon_x^s = -0.227 \times 10^{-3}; \quad \varepsilon_{y_s}^s = 0.227 \times 10^{-3}$$

$$\gamma_{xy}^s = -0.038 \times 10^{-3}$$

Step 5: Secant Moduli

1. Concrete—given

$$\varepsilon_{c1} = 2.094 \times 10^{-3}; \quad \varepsilon_{c2} = -0.288 \times 10^{-3}$$

$$f_{c1} = 1.08 \text{ MPa}; \quad f_{c2} = -4.93 \text{ MPa}$$

Find, using (5)

$$\bar{E}_{c1} = 516 \text{ MPa}; \quad \bar{E}_{c2} = 17{,}096 \text{ MPa}; \quad \bar{G}_c = 501 \text{ MPa}$$

2. Reinforcement—given

$$\varepsilon_{sx} = 0.597 \times 10^{-3}; \quad \varepsilon_{sy} = 1.208 \times 10^{-3}$$

$$f_{sx} = 119 \text{ MPa}; \quad f_{sy} = 242 \text{ MPa}$$

Using (7), find

$$\bar{E}_{sx} = 200{,}000 \text{ MPa}; \quad \bar{E}_{sy} = 200{,}000 \text{ MPa}$$

Step 6: Material Stiffness Matrices

1. Concrete—from (9) and (11), and with $\theta = 46.92°$

$$[D_c] = \begin{bmatrix} 5476 & 3885 & -4397 \\ & 4366 & -3875 \\ & & 4385 \end{bmatrix} \text{ (MPa)}$$

2. Reinforcement—from (10) and (11), given that ρ_1 = 0.01785, ρ_2 = 0.00713, $\alpha_1 = 0°$, and $\alpha_2 = 90°$, find

$$[D_s]_1 = \begin{bmatrix} 3570 & 0 & 0 \\ 0 & 0 & 0 \\ 0 & 0 & 0 \end{bmatrix} \text{ (MPa)}$$

$$[D_s]_2 = \begin{bmatrix} 0 & 0 & 0 \\ 0 & 1426 & 0 \\ 0 & 0 & 0 \end{bmatrix} \text{ (MPa)}$$

3. Composite

$$[D] = \begin{bmatrix} 9046 & 3885 & -4397 \\ & 5792 & -3875 \\ & & 4385 \end{bmatrix} \text{ (MPa)}$$

Step 7: Offset Strains

$$[\varepsilon_c^0] = [\varepsilon_c^p] = [\varepsilon_s^0]_1 = [\varepsilon_s^0]_2 = \{0 \quad 0 \quad 0\}$$

$$[\varepsilon^s] = \{-0.227 \quad 0.227 \quad -0.038\} \times 10^{-3}$$

In the NLFEA procedure, use $[\varepsilon^s]$ to determine the prestrain joint forces. Alternatively, at the element level, use (3) to determine the element prestress vector

$$(\sigma^\circ) = [D_c][\varepsilon^s] = \{-0.194 \quad 0.256 \quad -0.048\} \text{ (MPa)}$$

Step 8: New Estimate of Strains

From the NLFEA algorithm, determine the resulting strains at the conclusion of the 11th iteration

$$[\varepsilon]' = \{0.596 \quad 1.209 \quad 2.339\} \times 10^{-3}$$

$$[\varepsilon_c]' = \{0.823 \quad 0.982 \quad 2.377\} \times 10^{-3}$$

Alternatively, at the element level, use (2) to determine the new estimate of total strains

$$[\varepsilon]' = [D]^{-1}\{[\sigma] + [\sigma^\circ]\} = \{0.596 \quad 1.209 \quad 2.339\} \times 10^{-3}$$

$$[\varepsilon_c] = [\varepsilon] - [\varepsilon^s] = \{0.823 \quad 0.982 \quad 2.377\} \times 10^{-3}$$

where

$$[D]^{-1} = \begin{bmatrix} 0.215 & 0.000 & 0.216 \\ 0.000 & 0.422 & 0.373 \\ 0.216 & 0.373 & 0.775 \end{bmatrix} \times 10^{-3} \text{ (MPa}^{-1}\text{)}$$

$$[\sigma] = \{0.0 \quad 0.0 \quad 3.0\} \text{ (MPa)}$$

APPENDIX II. REFERENCES

Kollegger, J., and Mehlhorn, G. (1990). "Experimentelle Untersuchungen zur Bestimmung der Druckfestigkeit des gerissenen Stahlbetons bei einer Querzugbeanspruchung." *Rep. 413*, Deutscher Ausschuss für Stahlbeton, Berlin (in German).

Kuzmanovic, S. (1998). "An investigation of the shear design of a reinforced concrete box structure." MASc thesis, University of Toronto, Toronto.

Lefas, I. D., Kotsovos, M. D., and Ambraseys, N. N. (1990). "Behaviour of reinforced concrete structural walls: Strength, deformation characteristics and failure mechanism." *ACI Struct. J.*, 87(1), 23–31.

Okamura, H., and Maekawa, K. (1991). *Nonlinear analysis and constitutive models of reinforced concrete*, ISBN 7655-1506-0, University of Tokyo, Tokyo.

Shirai, S., and Noguchi, H. (1989). "Compressive deterioration of cracked concrete," *Proc., ASCE Struct. Congress 1989: Design, analysis, and testing*, ASCE, New York, 1–10.

Vecchio, F. J. (1990). "Reinforced concrete membrane element formulations." *J. Struct. Engrg.*, ASCE, 116(3), 730–750.

Vecchio, F. J. (1992). "Finite element modeling of concrete expansion and confinement." *J. Struct. Engrg.*, ASCE, 118(9), 2390–2406.

Vecchio, F. J. (1999). "Analysis of shear-critical reinforced concrete beams." *ACI Struct. J.*, 97(1), 102–110.

Vecchio, F. J. (2000). "Disturbed stress field model for reinforced concrete: Formulation." *J. Struct. Engrg.*, ASCE, 126(9), 1070–1077.

Vecchio, F. J., and Collins, M. P. (1982). "Response of reinforced concrete to in-plane shear and normal stresses." *Rep. No. 82-03*, Dept. of Civ. Engrg., University of Toronto, Toronto.

Vecchio, F. J., and Collins, M. P. (1986). "The modified compression field theory for reinforced concrete elements subjected to shear." *ACI J.*, 83(2), 219–231.

Walraven, J. C. (1981). "Fundamental analysis of aggregate interlock." *J. Struct. Div.*, ASCE, 107(11), 2245–2270.

APPENDIX III. NOTATION

The following symbols are used in this paper:

a = aggregate size (mm);
$[D]$ = total material stiffness matrix;

$[D_c]$ = material stiffness matrix for concrete component;
$[D_s]$ = material stiffness matrix for reinforcement component;
E_c = initial modulus of elasticity of concrete;
$\bar{E}_{c1}$ = secant modulus of concrete in principal 1-direction;
$\bar{E}_{c2}$ = secant modulus of concrete in principal 2-direction;
E_s = elastic modulus of reinforcing steel;
E_{sh} = strain hardening modulus of reinforcing steel;
$[F_c^s]$ = equivalent nodal forces representing offsets due to crack slip;
f_c' = compressive strength of concrete cylinder (28 days);
f_t' = tensile strength of concrete;
f_{cc} = compressive strength of concrete cube;
f_{c1} = principal tensile stress in concrete (in 1-direction);
f_{c2} = principal compressive stress in concrete (in 2-direction);
f_p = peak compressive stress in cracked concrete (negative value);
f_s = average stress in reinforcement;
f_{scr} = local stress (at crack) in reinforcement;
f_y = yield stress of reinforcement;
$\bar{G}_c$ = secant shear modulus of cracked concrete;
G_f = fracture energy of concrete;
$[k]$ = element stiffness matrix;
$[r_c^s]$ = equivalent free nodal displacements due to crack slip offsets;
s = average crack spacing in 1-direction;
s_x = average crack spacing in reference x-direction;
s_y = average crack spacing in reference y-direction;
$[T]$ = rotation transformation matrix;
v_c = shear stress on concrete relative to reference x,y-directions;
v_{ci} = shear stress on crack surface;
$v_{c\max}$ = maximum shear stress that can be resisted on crack surface;
w = average crack width;
α = inclination of reinforcement component relative to reference x-direction;
β_d = strength reduction factor due to transverse cracking;
γ_s = shear strain due to slip along crack surface;
$\Delta\varepsilon_{1cr}$ = local incremental strain in 1-direction at crack location;
$\Delta\theta$ = angle difference between inclinations of principal stresses and apparent principal strains;
δ_s = slip displacement along crack surface;
$[\varepsilon]$ = apparent (total) average strains in element, including crack slip strains;
$[\varepsilon_c^p]$ = plastic offset strains in concrete due to loading history;
$[\varepsilon^s]$ = equivalent average strains due to discontinuous slip along crack;
$[\varepsilon_c^0]$ = elastic offset strains in concrete due to expansion, thermal, or prestressing effects;
ε_s^0 = initial elastic prestraining reinforcement;
$[\varepsilon_c]$ = average strains in concrete, net of crack slip strains;
ε_{cr} = cracking strain of concrete;
ε_{c1} = strain in concrete in principal tensile stress direction;
ε_{c2} = strain in concrete in principal compressive stress direction;
ε_p = compressive strain at peak stress f_p in transversely cracked concrete (negative value);
ε_s = average strain in reinforcement;
ε_{scr} = local strain in reinforcement at crack location;
ε_{sh} = strain in reinforcement at start of strain hardening;
ε_u = ultimate strain for reinforcement;
ε_0 = compressive strain at peak stress f_c' in concrete cylinder (negative value);
θ = inclination of normal to crack direction in concrete;
θ_{ic} = inclination of principal stresses in concrete at first cracking;
θ_n = angle between reinforcement component and normal to crack;
θ_ε = inclination of apparent (total) principal strains in concrete;
θ_σ = inclination of principal stresses in concrete;
ρ = reinforcement ratio; and
$[\sigma]$ = average stresses acting on element.